Gondwana Research 67 (2019) 172–186

Contents lists available at ScienceDirect

Gondwana Research

journal homepage: www.elsevier.com/locate/gr

GR Focus Review

Modelling the long-term carbon cycle, atmospheric CO_2, and Earth surface temperature from late Neoproterozoic to present day

Benjamin J.W. Mills [a,*], Alexander J. Krause [a], Christopher R. Scotese [b], Daniel J. Hill [a], Graham A. Shields [c], Timothy M. Lenton [d]

[a] School of Earth and Environment, University of Leeds, Leeds LS2 9JT, UK
[b] Department of Earth and Planetary Sciences, Northwestern University, Evanston, IL 60201, USA
[c] Department of Earth Sciences, University College London, Gower Street, London WC1E 6BT, UK
[d] Global Systems Institute, University of Exeter, Exeter EX4 4QE, UK

ARTICLE INFO

Article history:
Received 31 May 2018
Received in revised form 21 November 2018
Accepted 6 December 2018
Available online 11 December 2018

Handing Editor: M. Santosh

Keywords:
Carbon cycle
Modelling
Paleoclimate
Biogeochemistry
Tectonics

ABSTRACT

Over geological timescales, CO_2 levels are determined by the operation of the long term carbon cycle, and it is generally thought that changes in atmospheric CO_2 concentration have controlled variations in Earth's surface temperature over the Phanerozoic Eon. Here we compile independent estimates for global average surface temperature and atmospheric CO_2 concentration, and compare these to the predictions of box models of the long term carbon cycle COPSE and GEOCARBSULF.

We find a strong relationship between CO_2 forcing and temperature from the proxy data, for times where data is available, and we find that current published models reproduce many aspects of CO_2 change, but compare poorly to temperature estimates. Models are then modified in line with recent advances in understanding the tectonic controls on carbon cycle source and sink processes, with these changes constrained by modelling $^{87}Sr/^{86}Sr$ ratios. We estimate CO_2 degassing rates from the lengths of subduction zones and rifts, add differential effects of erosion rates on the weathering of silicates and carbonates, and revise the relationship between global average temperature changes and the temperature change in key weathering zones.

Under these modifications, models produce combined records of CO_2 and temperature change that are reasonably in line with geological and geochemical proxies (e.g. central model predictions are within the proxy windows for >~75% of the time covered by data). However, whilst broad long-term changes are reconstructed, the models still do not adequately predict the timing of glacial periods. We show that the $^{87}Sr/^{86}Sr$ record is largely influenced by the weathering contributions of different lithologies, and is strongly controlled by erosion rates, rather than being a good indicator of overall silicate chemical weathering rates. We also confirm that a combination of increasing erosion rates and decreasing degassing rates over the Neogene can cause the observed cooling and Sr isotope changes without requiring an overall increase in silicate weathering rates.

On the question of a source or sink dominated carbon cycle, we find that neither alone can adequately reconstruct the combination of CO_2, temperature and strontium isotope dynamics over Phanerozoic time, necessitating a combination of changes to sources and sinks. Further progress in this field relies on $>10^8$ year dynamic spatial reconstructions of ancient tectonics, paleogeography and hydrology. Whilst this is a significant challenge, the latest reconstruction techniques, proxy records and modelling advances make this an achievable target.

Contents

* Corresponding author.
E-mail address: b.mills@leeds.ac.uk (B.J.W. Mills).

https://doi.org/10.1016/j.gr.2018.12.001

1. Introduction

Atmospheric carbon dioxide appears to have been essential in the maintenance of habitable conditions throughout Earth history by providing additional radiative forcing under a less luminous ancient sun. CO_2-related climatic stabilization is attributed to the feedbacks between planetary surface temperature and the long-term carbon cycle, which allow atmospheric CO_2 to increase in response to global cooling, and decrease in response to warming, over timescales of >100 kyrs (Walker et al., 1981; Kasting, 1989).

Simple 'box' models of the long-term carbon cycle have been developed to demonstrate and test these ideas against known temperature and CO_2 variations over the Phanerozoic Eon (Berner et al., 1983; Berner, 1991, 1994; Berner and Kothavala, 2001; Royer et al., 2004), and have been combined with models of other elemental cycles to also estimate concentrations of atmospheric oxygen, ocean sulphate and the behaviour of geochemical tracers such as $\delta^{13}C$ of carbonates and $\delta^{34}S$ of sulphates (Bergman et al., 2004; Berner, 2006; Arvidson et al., 2006).

The most recent Earth system box models are powerful predictive tools, used to reconstruct changes in global biogeochemistry and climate for times when proxy estimates are either unavailable or unreliable (Arvidson et al., 2013; Royer et al., 2014; Mills et al., 2016; Lenton et al., 2018; Krause et al., 2018), or used as a framework in which to test hypotheses about processes driving climate or biosphere changes over geological timescales (e.g. Falkowski et al., 2005; Mills et al., 2011; Boyle et al., 2014; Schachat et al., 2018; Lenton et al., 2018).

In this paper we return to the core predictions of Earth system box models, for atmospheric CO_2 and global surface temperature. These are among the most easily-testable predictions, as a wealth of pCO_2 estimates exist (Royer, 2014) and during the Cenozoic at least, surface temperature proxies are able to produce signals beyond the inherent uncertainties and climatic noise (e.g. Zachos et al., 2001; Hansen et al., 2013). In the following sections we attempt to construct broad estimates for both global average surface temperature and atmospheric CO_2 concentration over the Phanerozoic and beyond, given the available information. We then test current Earth system box models against these constraints, and those provided by the geological strontium isotope record, which responds to changes in the carbon cycle. Finally, we modify current models to take into account recent revisions of tectonic forcings, revise the strength of model feedbacks, and extend predictions back into the Neoproterozoic.

2. Global average surface temperature record

2.1. Whole Phanerozoic $\delta^{18}O$ record

Throughout this work we will seek to compile and model the changes to Earth's global average surface temperature, noting that an agreed record of global average surface temperature for the Phanerozoic Eon does not currently exist. The only current continuous Phanerozoic dataset pertaining to planetary temperature is the oxygen isotope composition of marine shells (Veizer et al., 1999; Veizer and Prokoph, 2015). However, the record shows a long-term trend towards more negative values further back in time. Fig. 1A shows low latitude brachiopod and planktonic foraminifera oxygen isotope data from the compilation of Veizer and Prokoph (2015), and the black line in Fig. 1B shows global average surface temperature estimates by assuming a linear relationship between $\delta^{18}O$ and local seawater temperature (Visser et al., 2003; see Supplementary File), and converting to global average surface temperature by assuming a scaling factor of 1.5 between low latitude and global temperature changes (Hansen et al., 2008).

Despite the trend towards more negative values, and thus higher temperatures, the low latitude oxygen isotope record shows cooling periods that agree very well with the timings of geological evidence for glaciation (Veizer et al., 2000). The record has been de-trended by assuming a gradual evolution of the oxygen isotope composition of seawater over the Phanerozoic following either a linear (Veizer et al., 2000) or quadratic (Veizer and Prokoph, 2015) function, and these corrections are applied in Fig. 1B. Much debate surrounds this dataset (Royer et al., 2004; Shaviv and Veizer, 2004; Grossman, 2012; Veizer and Prokoph, 2015; Bernard et al., 2017), and no clear mechanism has been defined to explain the proposed evolution of ocean $\delta^{18}O$ values, although it is known that hydrothermal processes can cause fractionation (Gregory and Taylor, 1981), as can changes to ice mass. Here we take the de-trended records as a starting point, and compare these to other independent estimates.

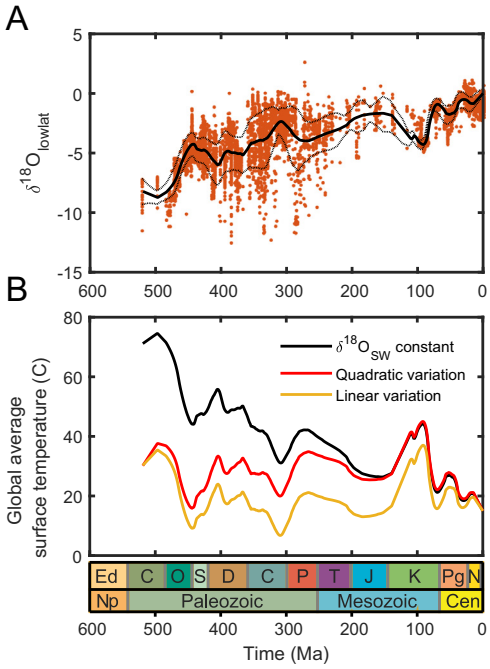

Fig. 1. Phanerozoic temperature estimated from low latitude oxygen isotopes. A. $\delta^{18}O$ record from planktonic foraminifera and brachiopods after Veizer and Prokoph (2015), black curve is a LOESS fit with a span of 10%, dashed lines show ±1 st. dev. B. Estimates for global average surface temperature from above record (see text), assuming the temperature function of Visser et al. (2003) and a seawater $\delta^{18}O$ value that is constant (black), or increases quadratically (red) or linearly (yellow) over the Phanerozoic (e.g. Veizer and Prokoph, 2015; Veizer et al., 2000). Global average temperature change is assumed to be 1.5× tropical temperature change (Hansen et al., 2008).

2.2. Mesozoic and Cenozoic temperature proxies

Earth surface temperature estimates are a commonly-used and seemingly-reliable metric in studies of Cenozoic climate change (Hansen et al., 2013). A detailed oxygen isotope record from benthic foraminifera (Zachos et al., 2001) has been instrumental in defining climate events such as the Paleocene-Eocene Thermal Maximum (PETM) and Early Eocene Climatic Optimum (EECO) (Zachos et al., 2008). A recent combined record of benthic foraminiferal $\delta^{18}O$ (Friedrich et al., 2012), including data for the Cretaceous, is reproduced in Fig. 2A. Temperature estimates from the smoothed record are plotted in Fig. 2B, following the formula in Hansen et al. (2013; see Supplementary File), and compare well with the Cenozoic temperature record presented in that paper.

A recently-developed and potentially promising paleothermometer is the organic lipid tetraether index, TEX_{86} (Schouten et al., 2002). The relationship between TEX_{86} and sea surface temperature has been demonstrated for the present day ocean, although uncertainty remains in the response to dissolved oxygen concentrations (Qin et al., 2015). Fig. 2C plots TEX_{86} sea surface temperature reconstructions from low latitudes, as calculated by recent studies (Zhang et al., 2014; Inglis et al., 2015; O'Brien et al., 2017), alongside estimates based on Mg/Ca ratios (Evans et al., 2018). A comparison of the Mesozoic and Cenozoic records with the de-trended Phanerozoic $\delta^{18}O_{lowlat}$ record is shown in Fig. 2D, and defines three periods of elevated surface temperatures during the mid Cretaceous, early Paleogene and early Neogene. However, the magnitude of these changes is generally less than implied by the de-trended oxygen isotope record. Recent TEX_{86} measurements from early Jurassic cores (Robinson et al., 2017) indicate sea surface temperatures in excess of modern values, generally agreeing with the de-trended $\delta^{18}O_{lowlat}$ curve. The generally lower temperatures recorded by TEX_{86} may indicate mixing with deeper waters (e.g. Jonas et al., 2017).

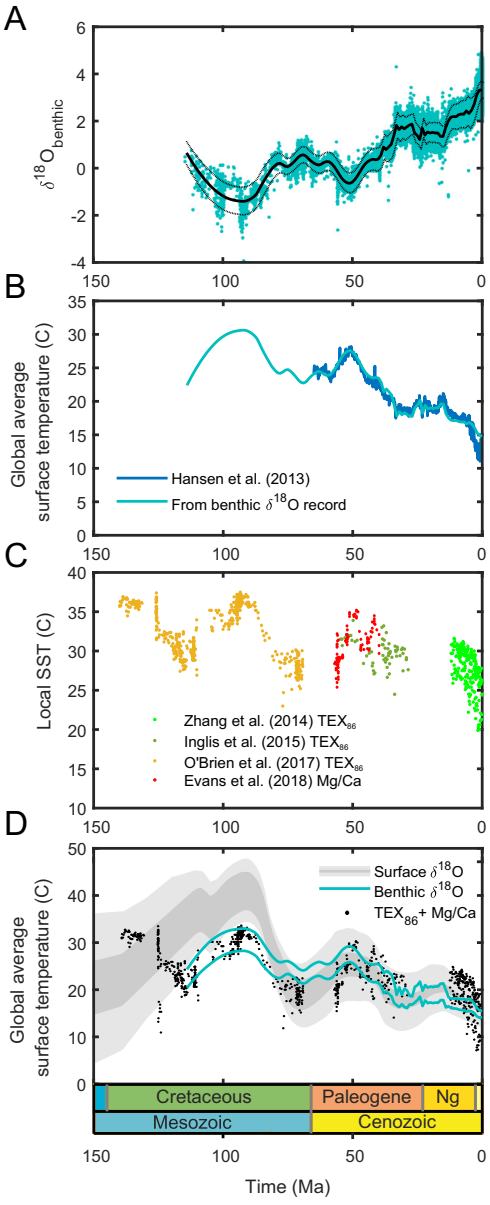

Fig. 2. Cretaceous and Cenozoic temperature change records. A. $\delta^{18}O$ record from benthic foraminifera after Friedrich et al. (2012). Black curve is a LOESS fit with a span of 30%. Dotted lines show ±1 st. dev. B. Global average surface temperature estimated from panel A (light blue), compared to recent temperature estimates from the Cenozoic portion of the record. C. Tropical sea surface temperatures from TEX_{86} paleothermometry and Mg/Ca ratios. D. Global average surface temperature comparison. The dark shaded area for $\delta^{18}O_{lowlat}$ shows the LOESS fit to data under the quadratic or linear variation in $\delta^{18}O_{seawater}$, and the lighter shaded area shows ±1 st. dev. For the benthic data, the blue lines encompass ±1 st. dev.

2.3. Glaciation ice line record

A commonly-used qualitative Earth surface temperature proxy is the paleolatitude of ice caps (Crowley, 1998; Royer et al., 2004). This record helps define the general oscillation between greenhouse (ice free) and icehouse (permanent ice cap) periods during the Phanerozoic and has been critical in the arguments presented for low-latitude 'snowball Earth' glaciations during the Neoproterozoic Era (Kirschvink, 1992; Hoffman et al., 1998). Simple one-dimensional energy balance models have been used to demonstrate the advance of ice caps towards the equator under either a decreasing solar flux, or decreasing concentration of atmospheric carbon dioxide (Budyko, 1969; Ikeda and Tajika, 1999; Hoffman and Schrag, 2002), and demonstrate a clear positive

relationship between the latitude of the ice line and the global average surface temperature, before reaching the 'snowball' instability.

It is clear that such models are extremely parameter-dependent and must make simplified approximations for heat transport between latitude bands that do not equate well to GCM models (Coakley and Wielicki, 1979). Thus, in order to examine the relationship between glaciation paleolatitude and global average surface temperature, we first plot the paleolatitude of glaciation (Crowley, 1998; Cather et al., 2009) and global average surface temperatures derived from benthic $\delta^{18}O$ for the Cenozoic in Fig. 3. These datapoints show a clear positive relationship and lie on a strong linear fit, allowing us to speculatively apply this metric to pre-Cenozoic ice line latitudes, as shown in Fig. 4. It is important to stress that this extrapolation involves uncertainty due to the differences in continental positions and ocean heat fluxes earlier in Earth history. Nevertheless, it is important to consider the quantitative implications of this proxy, given that it is widely used to define Phanerozoic greenhouse and icehouse climates. We find that the Paleozoic and Mesozoic temperature reconstructions using this method are in reasonable agreement with the area defined by the reconstructions in Sections 2.1 and 2.2.

Combining the ice-line temperature record with the paleothermometer indices described earlier allows us to tentatively define a broad window for global average surface temperature that encompasses all of these estimates (Fig. 4b). Here, the dark shaded area is derived from the $\delta^{18}O_{lowlat}$ record assuming either a linear or quadratic variation in $\delta^{18}O_{seawater}$, in combination with the ice line proxy for long glacial periods and the ± 1 st. dev. uncertainty in the benthic $\delta^{18}O$ record. The lighter shaded area represents the ± 1 st. dev. uncertainty in the $\delta^{18}O_{lowlat}$ record and encompasses the scatter in the TEX_{86} record and shorter-lived glacial periods. Much about the long term global temperature record remains uncertain and we see this reconstruction as embodying a multi-proxy 'best guess' that attempts to quantify the generally-understood long-term temperature changes over the Neoproterozoic and Phanerozoic. Broadly, the picture appears to be of temperatures below present day in the Cryogenian (Hoffman et al., 1998), rising to a Cambrian greenhouse, cooling towards the late Ordovician glaciation, hotter climates during the Silurian and early Devonian followed by a long descent into the Late Paleozoic Ice Age by around 300 Ma, then warm but fluctuating temperatures in the Mesozoic (e.g. Dera et al., 2011) and a long term cooling from the Cretaceous towards the present day.

3. Record of atmospheric CO_2 concentrations

3.1. Phanerozoic CO_2 proxies

A number of independent proxies have been developed to estimate atmospheric CO_2 concentrations over the Phanerozoic: The isotopic composition of carbon in carbonate minerals precipitated in paleosols, when combined with an estimate of soil-respired pCO_2 (Breecker et al., 2010), can be used to estimate atmospheric CO_2 concentration via a mass balance calculation (Cerling, 1984). The boron isotope ratio $\delta^{11}B$ can be used to estimate oceanic pH due to different isotopic compositions of the major boron species, which can then be used to estimate atmospheric CO_2 (Pearson and Palmer, 2000). The carbon isotope composition of carbon in phytoplankton organic alkenone molecules can be used to infer atmospheric CO_2, as fractionations generated by photosynthesis in the mixed layer depend to some degree on local DIC concentration, thermocline depth and nutrient availability (Jasper and Hayes, 1990; Pagani, 2002; Zhang et al., 2013). Finally, given that plant stomata respond to atmospheric pressure and CO_2, a Phanerozoic pCO_2 record can be derived from the fossil stomatal index, which measures stomatal density against epidermal cell density (Royer, 2001).

These proxy records have been carefully collated and summarised by Royer (2014), and the reader is directed to that paper for more information, including various critiques of the methods. The individual records from Royer (2014) are reproduced in Fig. 5 with moving averages shown as solid lines and standard deviations shown as light error bars. The lower panel shows a compilation of these CO_2 proxy records for the Phanerozoic, where the uncertainty window is a smoothed fit to the reported error window every 1 Myr. This window has a larger uncertainty range than the multiple-proxy LOESS fit of Foster et al. (2017), reflecting the divergent estimates between individual proxies, but is generally similar in shape.

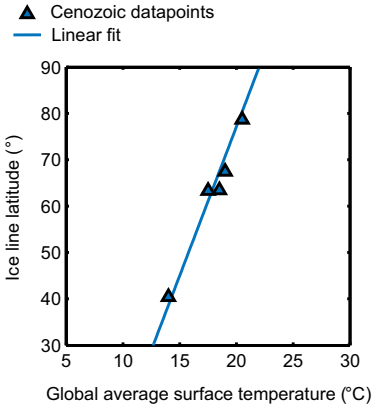

Fig. 3. Global average surface temperature and ice line latitude. Blue markers show relationship between paleolatitude of ice line and global average surface temperature for the Cenozoic, where temperature estimates are more certain (e.g. Hansen et al., 2013).

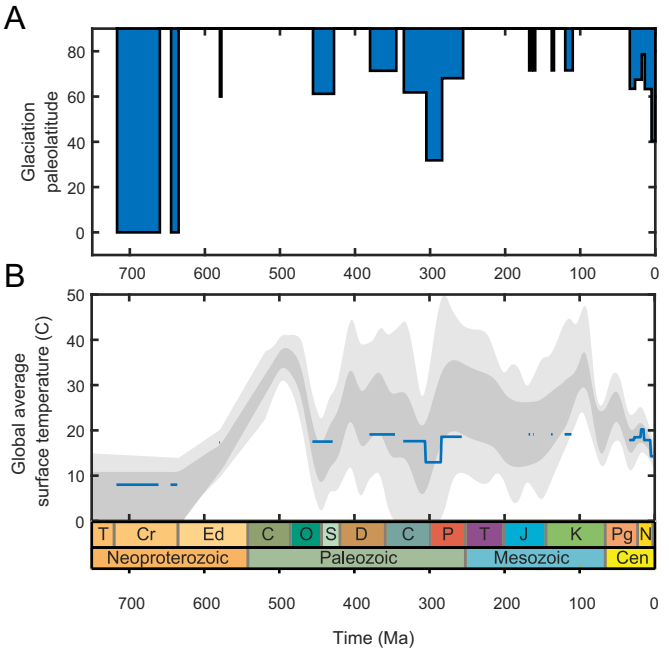

Fig. 4. Estimates of surface temperature from glaciation paleolatitude. A. Paleolatitude of glaciation (as compiled by Crowley, 1998; Cather et al., 2009). B. Estimated global average surface temperature for pre-Cenozoic time, using the relationship shown in Fig. 3. Grey area shows combined estimates from Figs. 1 and 2.

3.2. Relationship between Phanerozoic CO_2 and surface temperature

Having now compiled Phanerozoic CO_2 and temperature estimates, it seems worthwhile to directly investigate the apparent long-term climate sensitivity to changing CO_2 concentrations. The long-term climate sensitivity, or Earth System Sensitivity (ESS; Lunt et al., 2010) differs from the shorter term 'direct' climate sensitivity (e.g. Charney et al., 1979) by considering additional factors such as changes in land surface albedo, vegetation and hydrology. It is therefore expected to be

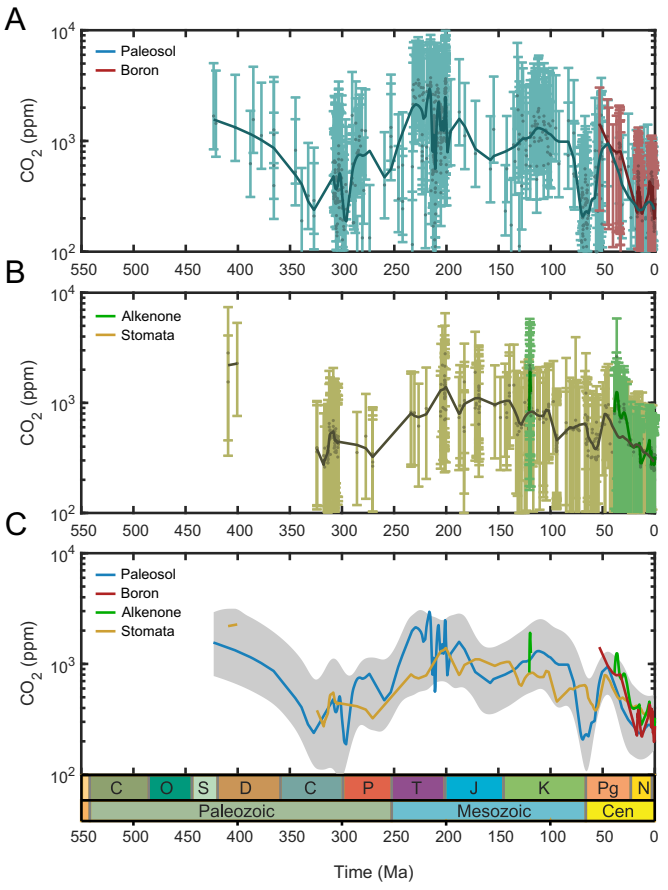

Fig. 5. Proxy estimates for atmospheric CO_2 concentration. A. Estimates from paleosols and Boron isotopes. B. Estimates from alkenones and stomatal indices. C. Mean estimates shown against grey area representing the average of the reported error windows.

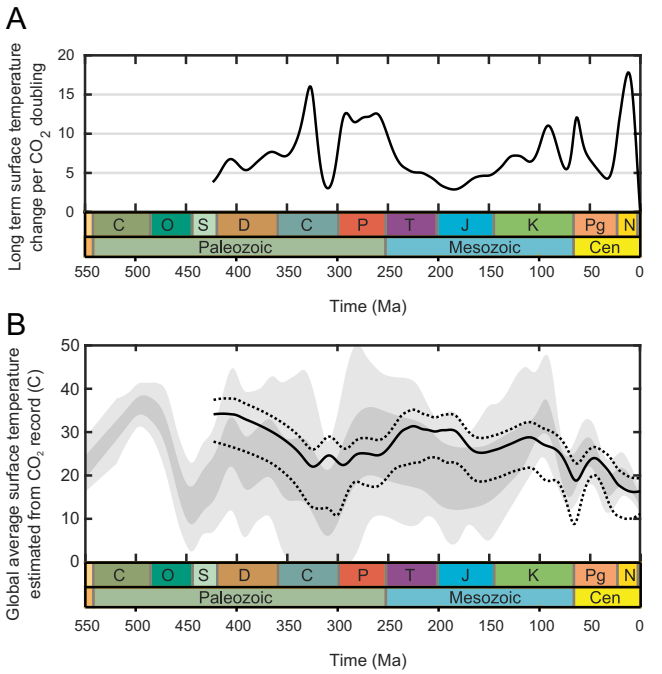

Fig. 6. Phanerozoic temperature and CO_2 relationships. Calculated from the GEOCARBSULF/COPSE temperature function (see text) which takes account of varying pCO_2 and solar luminosity (see text). A. Earth system sensitivity assuming medians of the CO_2 and temperature windows previously defined. B. Using proxy CO_2 to estimate global average surface temperature. Solid lines show median CO_2 estimate, dashed lines show min/max. Grey area shows proxy window from Fig. 4.

somewhere above the canonical 3 K per CO_2 doubling for the present-day Earth, and perhaps over 6 K per CO_2 doubling during glacial times (Royer, 2016).

To calculate the ESS for the dataset, we use the temperature function from the GEOCARBSULF and COPSE biogeochemical box models, which takes into account both the changes in solar luminosity and the CO_2 greenhouse (Berner, 2006; Royer et al., 2014; see Supplementary File). The results are shown in Fig. 6A. Estimated ESS oscillates around a value of around 5–10 K per CO_2 doubling, consistent with results of Royer (2016). Some very large sensitivities correspond in general with glacial periods, as might be expected due to ice-albedo positive feedback, but these also represent disagreements between the median CO_2 and temperature predictions over timescales <50 Myrs. That said, taking the median values of these two independent datasets confirms a clear positive correlation between CO_2 change and climate warming over the last ~420 Myrs (e.g. Royer et al., 2004). An important result is that one can use the CO_2 record to directly estimate temperature, using the GEOCARBSULF/COPSE function and a fixed ESS of 5 K, and produce results that agree reasonably well with the temperature proxy, as shown in Fig. 6B. The only clear disagreement here is during the Triassic-Jurassic, where proxy CO_2 concentration is high but surface temperature is relatively low. But even here, taking the lower bound of proxy CO_2 concentration produces temperature estimates towards the middle of the defined window. Therefore, there exists the possibility that models such as COPSE or GEOCARBSULF, in which the global average surface temperature is a function of only the solar flux and CO_2 greenhouse, may be able to competently reconstruct both of these metrics.

4. Earth system box models for the long-term carbon cycle

4.1. Carbon cycle processes and fluxes

A number of biogeochemical box models have been designed to calculate the transfer of carbon between the surface system (ocean plus atmosphere) and sediments, based on the scheme originally proposed in the GEOCARB model (Berner, 1991). This system considers a reservoir of surface CO_2 (atmospheric CO_2 plus ocean DIC), and much larger sedimentary reservoirs of buried carbonates (C_{carb}) and organic carbon (C_{org}). The major reservoirs and fluxes of the carbon cycle are shown in Fig. 7A, corresponding to the setup used in the most recent iteration of the COPSE model (Lenton et al., 2018).

In summary, long-term (>100 kyr) carbon inputs to the surface system occur through: direct mantle injection; the tectonic recycling and degassing of carbon-bearing sediments; and via the subaerial weathering of carbonates or fossil organic carbon. Long-term outputs from the surface system to the sediments occur via burial of organic carbon and precipitation of marine carbonates. The blue arrows in Fig. 7A show the supply of cations (e.g. Ca^{2+}, Mg^{2+}) from terrestrial silicate weathering and from seafloor hydrothermal alteration ('seafloor weathering'), which contribute to overall marine carbonate burial.

Carbon cycle models aim to reconstruct variations in the surface system CO_2 reservoir by reconstructing the magnitude of all input and output fluxes over geological timescales. Fluxes are estimated by considering 'forcings' and internal variables. Forcings are primarily tectonic and evolutionary changes and are imposed on the model, whilst internal variables are quantities such as pCO_2 and surface temperature, which the model is free to calculate over time. Both forcings and variables may influence model fluxes.

In this paper we will mostly experiment with the COPSE model, but we also run the latest version of GEOCARBSULF (Royer et al., 2014). These models are both based on the carbon cycle shown in Fig. 7A, and both also model the long-term geochemical cycles of sulphur and

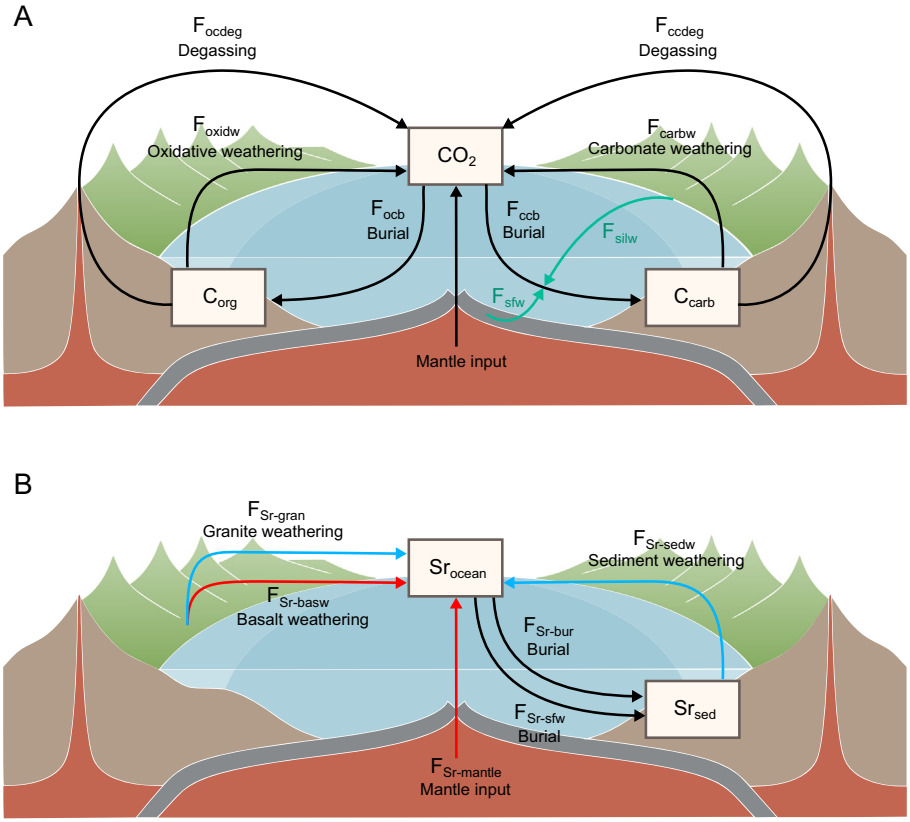

Fig. 7. Model representations of the long-term carbon and strontium cycles. A. Carbon cycle. Blue arrows show contribution of silicate weathering and seafloor weathering to total carbonate sequestration. B. Strontium cycle where blue arrows indicate inputs with high $^{87}Sr/^{86}Sr$ and red arrows indicate inputs with low $^{87}Sr/^{86}Sr$. Boxes show reservoirs and arrows show fluxes.

oxygen, but use very different treatments of the organic components of these cycles: COPSE calculates organic fluxes using built-in nutrient cycles (Van Cappellen and Ingall, 1994, 1996; Lenton and Watson, 2000a, 2000b), where the oceanic concentrations of phosphate and nitrate are free to vary and control primary productivity; GEOCARBSULF derives organic fluxes from the isotopic records of carbon and sulphur using a mass balance approach (Berner, 1987, 2001). There are also differences in the choice of model forcings, and the representation of model processes. Detailed reviews of both current models are available (Royer et al., 2014; Lenton et al., 2018) and the reader is directed to these papers for further discussion and model equations.

Despite the complexities of the carbon cycle, and of individual models, the regulation of atmospheric CO_2 concentration over the Phanerozoic is generally considered to be a balance between the overall CO_2 degassing rate, and the drivers of terrestrial silicate weathering rates (e.g. Berner, 2004). There are reasonably good reasons for this simplification: 1) carbonate (e.g. limestone) weathering is a source of surface system CO_2, but the products of weathering recombine over long timescales (>1 Myr) to form marine carbonates, 2) steady state for atmospheric oxygen requires steady state of the organic side of the carbon cycle (or an unsustainable imbalance in the sulphur cycle), 3) the rate of seafloor weathering appears to be controlled by ocean temperature and ridge generation rate, leaving it without an independent forcing (a 'slave variable').

4.2. Strontium cycle

The cycle of strontium is closely linked to the inorganic carbon cycle: strontium is delivered to the ocean following the weathering of silicates and carbonates, and substitutes for calcium during the formation of marine carbonates (Fig. 7B). For this reason, the Sr cycle has long been seen as a proxy for carbon cycle processes (Kump, 1989; Francois and Walker, 1992). Early studies tied variations in $^{87}Sr/^{86}Sr$ ratios to the weathering of different lithologies (e.g. Brass, 1976), but many modern works instead view Sr ratios as a balance between river input from terrestrial weathering (for which the isotope ratio is high) and from the mantle (for which the ratio is low) (Kennedy et al., 2006; Van Der Meer et al., 2014; Torres et al., 2014; Caves et al., 2016). Whilst river input is indeed more radiogenic, this interpretation is complicated by the differential weathering of highly radiogenic lithologies (carbonates, felsic silicates; blue lines in Fig. 7B; e.g. Galy et al., 1999), versus the weathering of less radiogenic basalts (Dessert et al., 2003; Allegre et al., 2010; red lines in Fig. 7B). The COPSE model includes a dynamic strontium cycle as shown in Fig. 7B, allowing it to output estimates of the seawater $^{87}Sr/^{86}Sr$ ratio over the Phanerozoic based on weathering rates, changes in lithology and mantle inputs (Francois and Walker, 1992; Mills et al., 2014; Lenton et al., 2018). Following similar reasoning, the GEOCARBSULF model uses the strontium isotope record to calculate the mafic fraction of terrestrial silicate weathering (Berner, 2008).

4.3. Published Phanerozoic reconstructions

Fig. 8 shows the Phanerozoic CO_2 and temperature reconstructions from the COPSE (Lenton et al., 2018) and GEOCARBSULF (Royer et al., 2014) models against the proxy estimates collated in earlier sections, and against the $^{87}Sr/^{86}Sr$ record (McArthur et al., 2012; Cox et al., 2016) for COPSE. Both models predict similar CO_2 concentrations for the Paleozoic Era, which fit reasonably well with proxies (Fig. 8A). Mesozoic CO_2 reconstructions from COPSE fall within proxy data, whilst GEOCARBSULF reconstructions are generally low. Neither model captures the apparent Paleogene maximum in pCO_2, with GEOCARBSULF underestimating pCO_2 at this time by >700 ppm, and requiring an extremely high degassing rate (~3× present day levels) to raise model estimates in line with geochemical proxies for this period (Royer et al.,

2014). A number of model parameters have high uncertainties, and it has been shown that a plausible change in the degree to which gymnosperm plants amplify silicate weathering rates may reconcile the GEOCARBSULF predictions for the Mesozoic (Royer et al., 2014).

In contrast to the CO_2 predictions, the global average surface temperature reconstructions of both models vary considerably less than inferred changes from proxy data (Fig. 8B). Average surface temperature in both models does not exceed 20 °C at any point during the Phanerozoic, and whilst generally low model temperatures during the Carboniferous-Permian agree with substantial glaciation at this time, the variation in temperature over the Cretaceous and Cenozoic bears little relation to the available direct estimates. This disagreement is a serious problem for these models, as the most recent ~100 Myr of Earth history contains the vast majority of available geochemical evidence. If a model bears no resemblance to the better constrained variations in temperature over the Cenozoic, then its predictions for the operation of the carbon cycle over deeper time should be treated with caution.

In the next section we investigate the possible reasons for the divergence of Earth system box models from available data. Basing our investigation firstly on the COPSE model, then exploring new versions of both COPSE and GEOCARBSULF. We revisit the model tectonic forcings, and the way in which weathering fluxes are linked to global erosion rates and temperature. We also take this opportunity to extend the COPSE model forcings back to 750 Ma. In the subsequent sections, 'unaltered models' refers to the most recent published COPSE (Lenton et al., 2018) and GEOCARBSULF (Royer et al., 2014) models.

5. Revisiting and extending model reconstructions

5.1. Tectonic forcings

Key forcings affecting the long-term carbon cycle are the relative rates of CO_2 degassing, and the relative rates of material uplift and erosion. In both the GEOCARBSULF and COPSE models, degassing rates are assumed to follow the rate of production at mid ocean ridges. This follows the reasoning that long-term plate creation and destruction rates are equal, and thus the ridge production rate is a proxy for both the rate of ridge CO_2 input and for the rate of subduction-recycling at volcanic arcs. GEOCARBSULF (Royer et al., 2014) uses the sea-level inversion of Gaffin (1987) to inform ridge production rates, whilst COPSE (Lenton et al., 2018) uses a simplified version of the Gaffin method (Mills et al., 2017) that is based on more recent sea-level reconstructions (Snedden and Liu, 2010; Haq, 2014).

The sea-level inversion method is unable to disentangle climate effects on the sea-level curve (Conrad, 2013), and an alternative method of reconstructing plate creation and destruction rates is through reconstructing the length of subduction zones. Subduction zone lengths have been reconstructed from direct imaging (Van Der Meer et al., 2014), plate tectonic reconstructions (Cao et al., 2017; Mills et al., 2017) and through kinematic modelling (Merdith et al., 2017) and show a general agreement over the last 750 Myrs (Mills et al., 2017). Under the assumption of a long-term, near-constant spreading rate, the rate of plate destruction, and therefore the total ridge and arc CO_2 input, should be reasonably approximated by the total global subduction zone length.

Recently it has been proposed that extensional tectonics, such as continental rifting, represents a significant and previously-ignored long-term CO_2 source, and it has been shown that basing the GEOCARBSULF model degassing rate on rift lengths produces a better fit to Paleogene CO_2 proxies than can be achieved using subduction zone lengths (Brune et al., 2017). Fig. 9A shows a record of global subduction zone length (from Mills et al., 2017 for 750–200 Ma and Van Der Meer et al., 2014 for 200–0 Ma), alongside the record of global rift lengths from Brune et al. (2017). Assuming that ~37% of tectonic CO_2 input is from continental rifts (Kelemen and Manning, 2015), and the rest is from ridges and arcs, we combine these curves to modify the CO_2 degassing forcing (assuming constant rift input before 200 Ma).

An additional subduction-related forcing in COPSE and GEOCARBSULF is the relative burial depth of carbonates. The evolution of pelagic calcifiers has likely increased the amount of carbonate entering subduction zones, increasing in turn the overall rate of CO_2 degassing (Volk, 1989). The current GEOCARBSULF model (Royer et al., 2014) assumes that this contribution to degassing rates has risen linearly over the period 150–0 Ma, and this formulation is used in the most recent COPSE model (Lenton et al., 2018). Given that the link between carbonate deposition and degassing is not straightforward (Edmond and Huh, 2003), and that both current models predict low temperature over the last 150 Myrs, we return this forcing to follow its original description (Berner, 1991), where it rises from a value of 0.75 at 150 Ma to reach the modern day value (of 1), by ~100 Ma.

Erosion rates in both COPSE and GEOCARBSULF are informed by a long-term polynomial fit to the sediment mass compilation of Ronov (1993) and erosion-loss relationship of Wold and Hay (1990). We extend this forcing back to 750 Ma using a moving average through an updated version of this data which includes Quaternary values (Hay et al., 2006), shown in Fig. 9B.

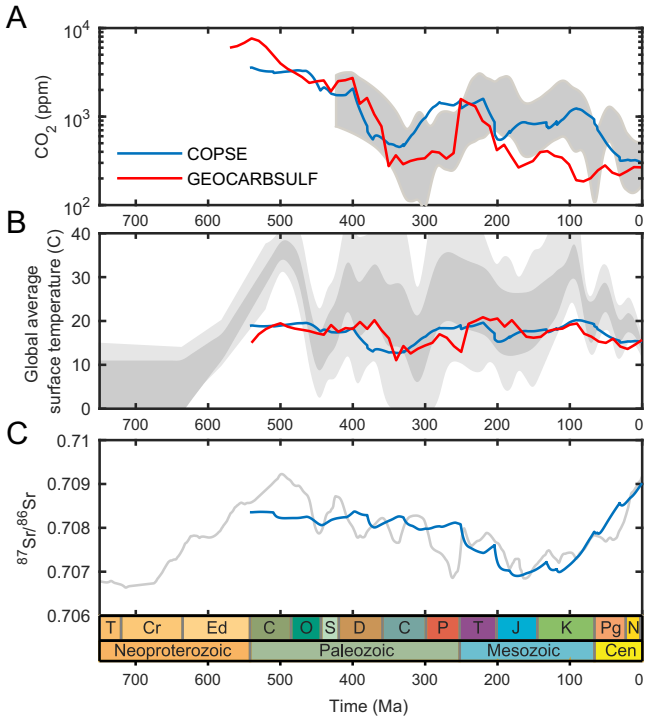

Fig. 8. Published box models for Phanerozoic CO_2 and surface temperature. A. Atmospheric carbon dioxide. B. Global average surface temperature. Grey areas show proxy estimates developed in earlier sections. Models shown are most recent versions of COPSE (Lenton et al., 2018) and GEOCARBSULF (Royer et al., 2014). C. Strontium isotope ratios. Grey line shows data of Cox et al. (2016) and McArthur et al. (2012).

5.2. Effect of erosion on weathering fluxes

Global rates of silicate weathering are estimated in box models from the global average surface temperature following Arrhenius' equation for the influence of temperature on chemical reaction rates, and scaling by the global rate of runoff, which is itself a function of average surface temperature (Berner, 1994). Aside from temperature and runoff, chemical weathering is also influenced by the supply of material from erosion, but the relationship between erosion rates and overall chemical weathering is complex. Low erosion rates limit chemical weathering, and a linear trend between physical and chemical weathering is observed in low-erosion catchments (West et al., 2005). High erosion

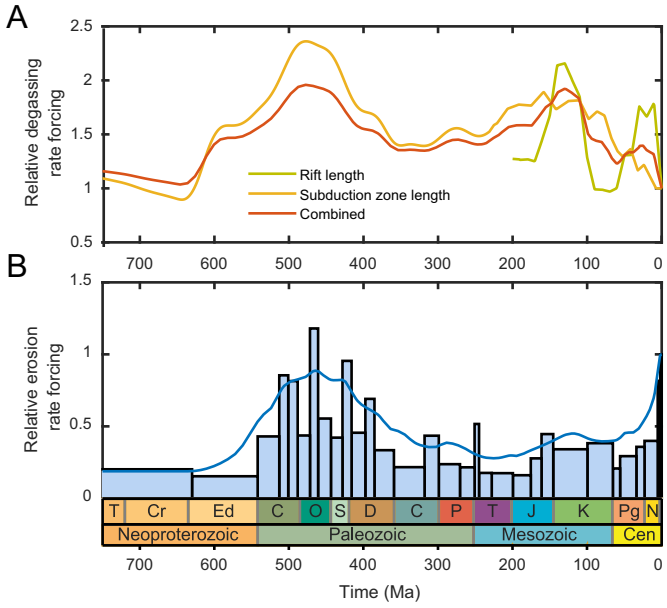

Fig. 9. Updated tectonic model forcings. A. Relative rate of CO_2 degassing calculated from lengths of subduction zones (Mills et al., 2017; Van Der Meer et al., 2014) and rifts (Brune et al., 2017; average of L1 and L2 reconstructions). B. Relative rate of continental erosion after Hay et al. (2006). Blue line shows 100 Myr moving average. See text for more information on both forcings.

rates permit greater rates of chemical weathering (Gaillardet et al., 1999), but there is no clear relationship between physical erosion and chemical weathering in high erosion catchments as the reaction rate is controlled by kinetics, rather than material availability (Gabet and Mudd, 2009; West, 2012). Additionally, as might be expected under kinetic control, high erosion rates favour the chemical weathering of more reactive lithologies such as carbonates, over less reactive silicates (e.g. Jacobson and Blum, 2003).

Box models aim to represent the global weathering flux in response to changing global variables, and thus the overall erosion rate is considered in terms of the abundance of mountainous weathering environments, rather than simply the erosion rate in a single catchment. The COPSE model therefore links the global rates of silicate and carbonate weathering directly to the overall relative erosion rate. Other models have differentiated between the effects of erosion on silicate and carbonate weathering (Li and Elderfield, 2013; Shields and Mills, 2017) and we follow this interpretation here, allowing carbonate weathering a near-linear relationship with erosion rates, and silicate weathering a weaker relationship (see Supplementary File).

5.3. Strength of weathering-temperature feedbacks

The current model reconstructions displayed in Fig. 8 show that both the COPSE and GEOCARBSULF models strongly regulate surface temperature at values close to the present day. This is chiefly because changes in global average surface temperature cause a change in the silicate weathering CO_2 sink, which buffers against the original temperature change by altering atmospheric CO_2 concentrations. Overly-strong temperature regulation in these models may be due to an overestimation of the effect of average surface temperature and runoff changes on globally-integrated weathering rates. This can occur because not all silicate weathering is kinetically limited, and temperature in low latitudes, where much of the present-day runoff and weathering occurs (e.g. Andes, Himalaya, Indonesia; Hartmann et al., 2014), varies less than the average global surface temperature due to polewards heat transport. In order to test weaker temperature feedbacks in COPSE, we define an effective weathering temperature. This is defined to be the temperature in the tropics, using the earlier defined ratio of 1:1.5 between tropical and global temperature changes proposed by Hansen et al. (2008).

5.4. COPSE model reconstructions for CO_2 and surface temperature from 750 Ma to present

Fig. 10 shows results of the COPSE model following the updates detailed in the previous sections. Panels A and B show model reconstructions where surface processes are driven by the global average temperature change, and panels C and D show model reconstructions where surface processes are driven instead by low latitude temperature change. We also run the model for a variety of Earth system temperature sensitivities to CO_2 (ESS, coloured lines). Changing the ESS alters the relationship between model CO_2 and surface temperature, and this effect is further enhanced when the CO_2 negative feedbacks are weakened by assuming that most chemical weathering occurs at low latitudes. Taking ESS = 5 K and using the low-latitude temperature change to drive surface reactions (green line in panels C and D) gives predictions of CO_2 and surface temperature that are largely within the combined proxy data, and we take this as the new COPSE model baseline.

5.5. GEOCARBSULF model reconstructions for CO_2 and surface temperature

Uncertainty about the operation of the Neoproterozoic carbon cycle currently prevents the GEOCARBSULF model being run beyond the Phanerozoic, as the isotope mass balance approach to calculating organic fluxes fails when the input carbonate $\delta^{13}C$ is below the mantle value of ~−5‰, such as during the enigmatic Shuram excursion (e.g. Rothman et al., 2003). Nevertheless, it is worthwhile to test our modifications to the COPSE model by applying them to GEOCARBSULF (Sections 5.1, 5.2, 5.3). We alter the degassing and erosion rate forcings for GEOCARBSULF to match the updated COPSE forcings, revise the relationship between uplift and weathering fluxes (which includes adding a dependency of carbonate weathering on uplift and erosion), and use the effective weathering temperature at low latitudes. We fix the Earth system temperature sensitivity, Γ, at 5 K per CO_2 doubling, as in COPSE. We also revise the forcing for 'the fraction of land undergoing chemical weathering' (f_{AW}/f_A), to normalise the forcing to the present day (as in Lenton et al., 2018).

In addition to these modifications, we also reconsider some recent changes to GEOCARBSULF: A number of forcings were revised by Royer et al. (2014) from the original Berner (2008, 2009) and Berner (2008, 2009) version of GEOCARBSULF, which alter model outcomes substantially, creating a larger discrepancy between the model and the proxy record. These forcings are: the total land area (f_A); the global runoff (f_D) due to changing paleogeography; the fraction of land undergoing chemical weathering (f_{AW}/f_A) and the global average continental temperature (*GEOG*) due to changing paleogeography. Additionally, the time invariant chemical weathering parameters: the rate of chemical weathering of volcanic, compared to non-volcanic, silicate rocks (*VNV*); the variability of the $^{87}Sr/^{86}Sr$ of granites over time (*NV*); and the rate of the basalt-seawater reaction at present ($f_B(0)$), are also revised by Royer et al. (2014). GEOCARBSULF is very sensitive to the above forcings, and further analysis (not shown) confirms that much of the variation in the two versions above comes from the *GEOG* and volcanic weathering parameters. In this work, we opt to revert all of the parameters discussed above to their descriptions in the earlier papers of Berner. This should not be seen as a refutation of the work of Royer et al., as we see these differing parameterisations as part of the model uncertainty and our goal here is to determine, within this uncertainty, whether or not the model can produce a reasonable reconstruction of Phanerozoic temperature and CO_2.

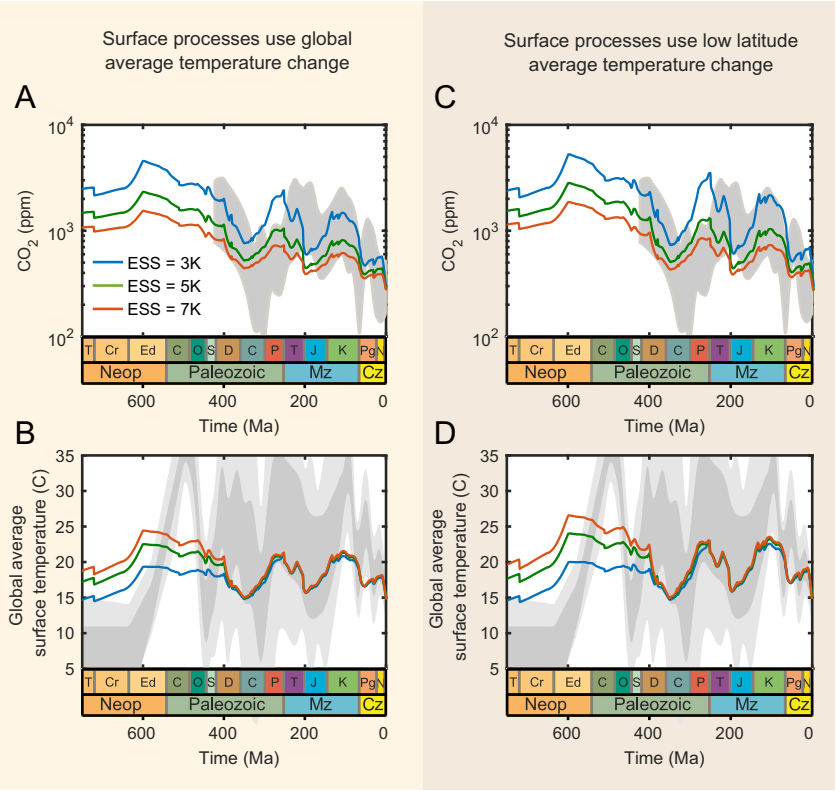

Fig. 10. COPSE model reconstructions of CO_2 and surface temperature. A and B show model reconstructions where weathering functions use global average surface temperature change. C and D show model reconstructions where weathering functions use low latitude temperature change instead. Coloured lines show different choices of Earth System Sensitivity (ESS).

5.6. Comparisons of revised COPSE and GEOCARBSULF models to Phanerozoic CO_2 and surface temperature records

Fig. 11 plots comparisons between the unaltered and revised COPSE and GEOCARBSULF models, and compares these to the uncertainty windows defined in this work for Phanerozoic global average surface temperature and atmospheric CO_2 concentration. We also employ some simple statistical tests of the ability of the models to simulate temperature and CO_2 records that are within the proxy limits: *%outbound* is a calculation of the percentage of the model output which falls outside the highest confidence windows for both temperature and CO_2 (the dark grey windows); *Total error* is the sum of the distances between the model outputs and the means through the proxy data windows. Both of these statistics are calculated from 1 Myr bins over 423–0 Ma, which defines the availability of the CO_2 proxy data, and covers the more reliable temperature reconstructions. If the model output is entirely contained within the proxy window then *%outbound* would be zero, and if the model output sits exactly on the data window mean then *Total error* is also zero. The CO_2-temperature data comparison in Fig. 6 shows that it is technically possible for *%outbound* to be zero for both CO_2 and temperature, but it is not possible for *Total error* to be zero in both cases, as there is some mismatch between the means of the CO_2 and temperature proxy windows.

For COPSE, the revised CO_2 predictions for the Paleozoic are broadly similar to the unaltered model, showing a decline from Cambrian to Carboniferous, followed by a rise to a peak around 250 Ma. CO_2 reconstructions for the Mesozoic and Cenozoic now display broad peaks in the Cretaceous and Paleogene, reasonably consistent with the long-term pattern shown in proxy data, with the difference driven primarily by the consideration of rift activity in the degassing rate of CO_2 (Brune et al., 2017). The statistical metrics plotted in Fig. 11C show no clear difference in the overall ability of the unaltered and revised COPSE models to stay within the data windows for CO_2, or to match the data means. However, revised COPSE model temperature reconstructions are significantly closer to proxy data than those of the unaltered model. Around 80% of the model output is now within the stricter temperature range, as opposed to <50% for the unaltered model. This is because the shape of the model CO_2 output now more closely resembles the changes in temperature, and the increased Earth System Sensitivity leads to a stronger relationship between CO_2 forcing and surface temperature. This is especially evident for Cretaceous to present. This level of detailed box modelling has not previously been run for the late Neoproterozoic, and the results here confirm the expected trend of increasing temperature between the Cryogenian and Ediacaran, which is largely due to the increase in CO_2 degassing rates (Mills et al., 2017). However, the model does not produce the level of Cambrian warmth implied by the available proxies for this time, and does not show any significant cooling associated with the Hirnantian glaciation in the late Ordovician. The model also produces a relatively warm Cryogenian, but a number of possibilities exist for further cooling at this time, including intense weathering of low-latitude flood basalts (Cox et al., 2016), or biologically-driven chemical weathering (Lenton and Watson, 2004).

The modified GEOCARBSULF model improves the fit to the proxy data substantially, and shows an evolution of pCO_2 that is almost entirely within the boundaries of the data compilation. For global average surface temperature, the modified GEOCARBSULF model has similar error metrics to the modified COPSE model, but is less able to reproduce the broad humps in temperature during the Cretaceous and Cenozoic. As discussed earlier, our modification of GEOCARBSULF also includes reverting some revisions made to that model by Royer et al. (2014). However, these revisions may represent an increased understanding of the processes themselves, and it is not acceptable to simply use the forcings and relationships that give the closest match to proxies if they are not supported by current research. The version of COPSE used in this paper does however incorporate the updated forcings for *fD* and f_{AW}/f_A, without resulting in very low temperature and CO_2

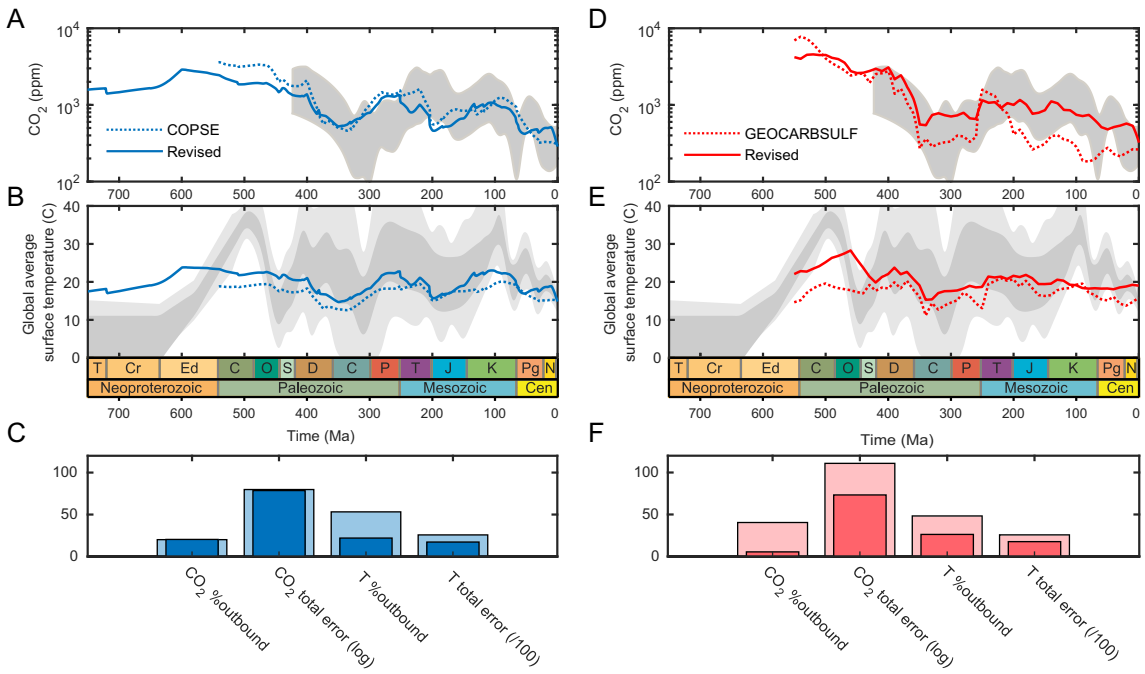

Fig. 11. Updated GEOCARBSULF and COPSE model reconstructions, compared to proxy data windows. A. COPSE atmospheric CO_2 concentration. B. COPSE global average surface temperature. Solid lines show revised model, dotted lines show unaltered model (e.g. the most recent published versions of Lenton et al. (2018) and Royer et al. (2014)). C. COPSE statistical tests. Dark bars show revised model, light bars show unaltered model. D–F show the same metrics for GEOCARBSULF. See text for details.

reconstructions for the Mesozoic and Cenozoic that are seen in the Royer et al. version of GEOCARBSULF. This can be attributed to the increased level of negative feedback in COPSE, which is a result of the dynamic biosphere and nutrient cycling in the model. Thus it appears that some key updated forcings and parameters in GEOCARBSULF could be consistent with the observed operation of the long-term carbon cycle, but only if the model were to also take biotic feedbacks into account. COPSE does not include the *GEOG* parameter that alters the continental temperature due to paleogeographic changes, and preliminary experiments to include this parameter degrade the model predictions, even with strong biotic feedbacks. Thus it may be the case that these changes to continental temperature do not affect chemical weathering in a way that is easily incorporated into a box model, or that other counterbalancing processes have not been considered.

5.7. Strontium cycling and $^{87}Sr/^{86}Sr$ from 750 Ma to present

The COPSE model reconstruction of seawater $^{87}Sr/^{86}Sr$ (Fig. 12A) is in reasonable agreement with long-term geological trends for the Phanerozoic (as was that in Lenton et al., 2018), and as in the previous model, is driven largely by changes in erosion rates. Fig. 12B shows a breakdown of the strontium fluxes from each model process. The changes in strontium input from the weathering of ancient silicates ('granite') and carbonates (both relatively radiogenic) are driven largely by the changing erosion rates.

The late Neoproterozoic $^{87}Sr/^{86}Sr$ reconstruction shows the same general trend as is observed in the data but cannot reproduce the magnitude of the rise between the Tonian and Cambrian. This is potentially due to uncertainty in the rates of basalt weathering for the late Neoproterozoic and Early Phanerozoic. In the model, the weathering of basalts depends on the amount of exposed mafic rocks, which is largely informed by records of Large Igneous Province (LIP) areas (Ernst, 2014; Mills et al., 2014). An apparent paucity of Precambrian and Paleozoic LIPs drives low and fairly stable basaltic area in the model, but may simply be a consequence of the decline in preserved crustal material with age. Future work could seek to correct for this effect.

Fig. 12C shows the ratio of strontium river inputs to mantle input. If all terrestrial Sr sources had the same isotopic composition (e.g. $^{87}Sr/^{86}Sr_{river}$ is constant) then this quantity would be expected to track the seawater $^{87}Sr/^{86}Sr$ reconstruction in Fig. 12A. This is clearly not the case, and especially so when considering only silicate weathering versus mantle input. The riverine strontium signal is a combination of at least three sources, each with their own distinct controls and isotopic signatures, and thus considerable caution is advised when considering any direct back-calculation from ocean $^{87}Sr/^{86}Sr$ to silicate weathering rates.

6. Summary and conclusions

6.1. Links between the long-term carbon cycle, CO_2, and Earth surface temperature

By compiling independent proxy records of global average surface temperature and atmospheric CO_2 concentration for the Phanerozoic, we have shown that when accounting for the solar flux, long-term Phanerozoic surface temperature changes can be clearly related to variations in the CO_2 greenhouse (Fig. 6). CO_2 appears to be a primary driver of climate on geological timescales (e.g. Royer et al., 2004).

Furthermore, the long-term CO_2 concentration derived from direct proxies agrees reasonably well with that predicted by biogeochemical box modelling at the Phanerozoic scale. This finding gives confidence that such models include broadly the right suite of processes, and accurately discern the relative importance of these in driving climate regulation. However, there are a number of instances where the models and proxies disagree, suggesting that either the current forcings remain poorly constrained, or additional processes become important at these times.

6.2. Model discrepancies: late Ordovician cooling

A key area of model-proxy disagreement is the apparent cooling and glacial period in the late Ordovician (Hirnantian). It has been proposed that a reduction in CO_2 concentration and temperature may be related to reductions in CO_2 degassing rates (based on lower abundances of

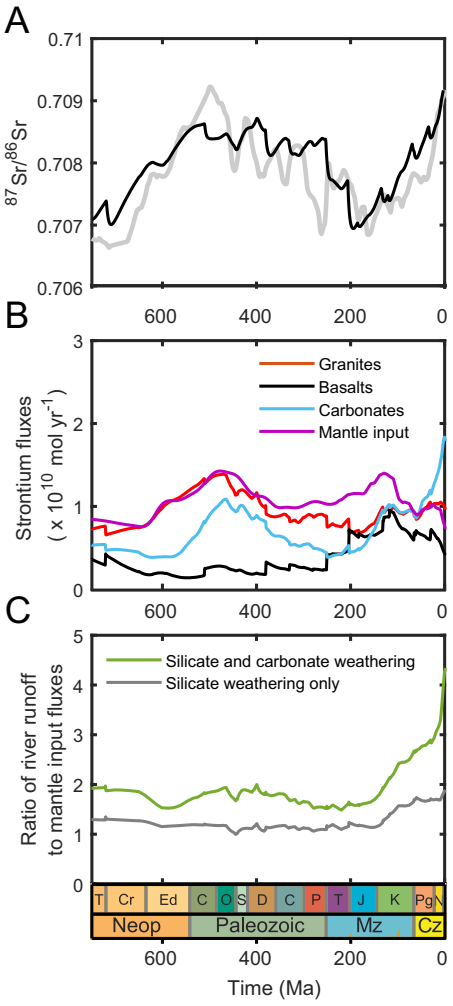

Fig. 12. COPSE model strontium system. A. Ocean $^{87}Sr/^{86}Sr$ isotope ratio (black), compared to data in grey. Black line shows 'reduced feedback' model with Earth System temperature sensitivity of 5 K. B. Model strontium fluxes. C. Ratios of strontium inputs from river runoff and mantle processes. Note that whilst the system produces a broad reconstruction of strontium isotope dynamics, this is not related to changes in overall silicate weathering rates.

young zircons, McKenzie et al., 2016), or to enhanced weathering of volcanic rocks (evidenced by a fall in seawater $^{87}Sr/^{86}Sr$, Young et al., 2009; Nardin et al., 2011). A reduction in degassing rates during the late Ordovician is not yet validated by any quantitative tectonic reconstruction (see Mills et al., 2017 for a compilation), and is not included in our model. There is also no clear evidence for a significant increase in volcanic weathering during this time, although this is clearly possible, given the tectonic events of the time (e.g. weathering of the Famatinian arc: Young et al., 2009).

Fig. 13 shows the COPSE model reconstruction for the late Ordovician, which predicts generally static and high global average temperatures and static $^{87}Sr/^{86}Sr$ (solid lines). Dashed and dotted lines show model runs that explore adding additional volcanic basalt weathering starting in the late Ordovician (from 450 to 430 Ma). The dashed lines show the effects of adding the entire present day basalt weathering area, and the dotted lines show the addition of twice this amount. Such an event might be best explained by the emplacement of a Large Igneous Province (LIP), as hypothesised for this time period (Lefebvre et al., 2010). Enhancing silicate weathering in this manner causes CO_2 and temperature to decline, and $^{87}Sr/^{86}Sr$ to fall (e.g. Fig. 7). In order to not exceed the amount of variation observed in ocean $^{87}Sr/^{86}Sr$, global cooling is limited to about 3 °C on average, or around 2 °C in the tropics – far below the degree of cooling proposed by examining

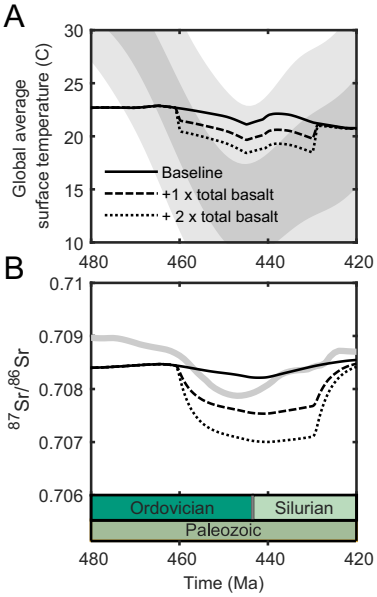

Fig. 13. COPSE model response to proposed late Ordovician LIP. A. Global average surface temperature. B. Seawater strontium isotope ratio. Solid lines show new baseline run. Dashed lines show the addition of the entire total present day basaltic area (e.g. roughly equal to CAMP eruption), dotted lines show addition of twice the modern basaltic area.

oxygen isotopes (Trotter et al., 2008). The rise of the first land plants greatly accelerating weathering, particularly of easily-weathered volcanic rocks (Lenton et al., 2012), combined with a 'tipping point' in sea-ice cover on the then ocean-covered Northern Hemisphere (Pohl et al., 2014) may be the best way to explain this sharp cold interval.

6.3. Reconciling box modelling with Neogene and Quaternary proxies

A persistent problem with long-term Phanerozoic modelling has been the inability to reproduce the events of the late Cenozoic. Due to the abundance of proxy data for CO_2 and temperature, and non-traditional isotopic proxies such as lithium and beryllium (Misra and Froelich, 2012; Willenbring and von Blanckenburg, 2010), the cooling period in the late Cenozoic has long been the testing ground for hypotheses about the long-term carbon cycle and regulation of Earth surface temperature (Raymo and Ruddiman, 1992).

Our modifications to the COPSE model produce a reasonable fit to Neogene and Quaternary records of global average surface temperature, atmospheric CO_2 concentration and ocean $^{87}Sr/^{86}Sr$ (Fig. 14). As noted earlier, they confirm the established (but frequently overlooked) view that late Cenozoic cooling does not require a long-term increase in silicate weathering rates (Kump and Arthur, 1997): The silicate weathering flux is set by the global carbon cycle balance, and increases in erosion result in this global balance being maintained at a lower temperature. A shift towards more positive $^{87}Sr/^{86}Sr$ values is the consequence of the weathering of uplifted older terranes and sediments during a period of generally increased erosion rates, but decreasing global rates of silicate weathering (as required by a decreasing CO_2 input rate).

6.4. A source and sink driven long-term carbon cycle

Recent studies have asked whether the long-term carbon cycle is primarily controlled by the carbon sources from CO_2 degassing (McKenzie et al., 2016), or by the changing carbon sink due to silicate weathering (Goddéris and Donnadieu, 2017). The COPSE model is well-placed to investigate this question. Fig. 15 shows 'source-only' and 'sink-only' versions of the model, in which the other forcings are kept at their present value. It should not be surprising that neither of

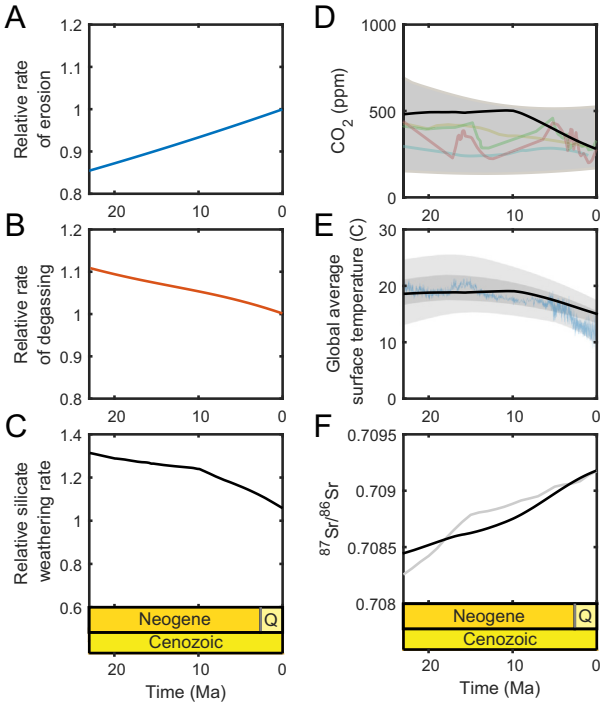

Fig. 14. COPSE model reconstruction of the Neogene carbon cycle. A. Relative erosion rate. B. Relative degassing rate. C. Relative rate of silicate weathering. D. Atmospheric carbon dioxide concentration. Individual mean estimates and overall uncertainty window as in Fig. 5. E. Global average surface temperature. Benthic foraminiferal estimates and overall uncertainty window as in Figs. 2 and 4. F. Seawater strontium isotope ratio. As per Fig. 12, increasing strontium isotope ratios can occur under decreasing silicate weathering rates.

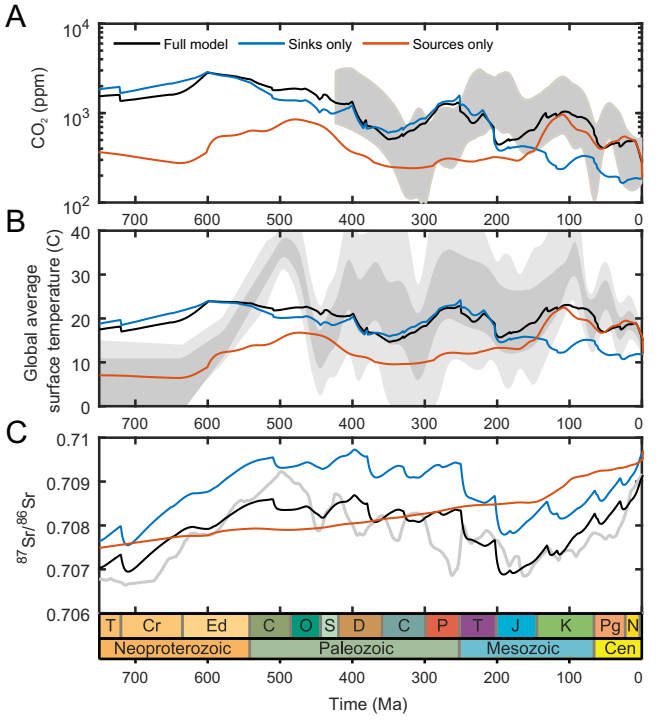

Fig. 15. Source and sink driven models. COPSE model run with constant CO_2 sources and varying sinks (blue), or vice-versa (red). A. Atmospheric carbon dioxide concentration. B. Surface temperature. C. Seawater strontium isotope ratios.

these models can reproduce the general long-term climate trends of the full model, as model development aims to only include the most relevant processes (see Lenton et al., 2018).

In agreement with Goddéris and Donnadieu (2017), the sink-only model can explain climate shifts before the Jurassic reasonably well, but not during the Cretaceous and Cenozoic. The source-only model can explain the general trend in temperature increases and decreases, and can do so quite well if the burial depth of carbonates ('B forcing') is ignored. However, the source-only model cannot explain variations in ocean $^{87}Sr/^{86}Sr$. Whilst strontium isotope ratios are not a direct weathering proxy, their variations are primarily controlled by changes in carbon sinks. Thus, a source-driven carbon cycle cannot be made consistent with the $^{87}Sr/^{86}Sr$ record.

6.5. Spatial weathering regimes and the future of box modelling

Estimating long-term chemical weathering rates in a nondimensional box model is a difficult task. The global rates of chemical weathering on the present-day Earth are spatially heterogeneous (e.g. Hilley and Porder, 2008; Hartmann et al., 2014), and depend on local temperature, and rates of erosion and runoff (Gaillardet et al., 1999; West, 2012). A reasonable marriage of these parameters can be achieved in spatial models in order to estimate global silicate weathering rates and CO_2 drawdown for snapshots of the ancient carbon cycle, with impressive results (Goddéris et al., 2012, 2014, 2017), but the number of computer CPU hours required to solve these models means that they have not been used to create continuous 500-million year records of isotope tracers, or represent non-steady-state dynamics, such as the build-up of carbon in the Earth's crust and long-term exchanges with the mantle (Hayes and Waldbauer, 2006). Long integration times also affect model development and testing, limiting the number of experiments that can be run.

There is scope to move beyond the current situation. One approach would be to asynchronously couple between running 'snapshots' of a climate model to derive spatially-explicit weathering fluxes and using a box model to span much longer intervals between the snapshots. More economically, if for a given paleogeography it can be established from the climate model that the spatial pattern of precipitation changes scales with global average temperature – as is the case for the modern climate – then a pattern-scaling approach can be taken (Huntingford et al., 2010; Huntingford and Cox, 2000). In this approach the spatial pattern of precipitation and how it changes with global temperature would be extracted from a climate model for a series of snapshots through the Phanerozoic, and then an elaborated box model would use these scaled patterns to drive weathering fluxes. This would provide a computationally efficient solution, but still poses some issues such as how to incrementally change between different paleo-geographies during the operation of plate tectonics.

In conclusion, recent advances in reconstructing tectonic drivers of the long-term carbon cycle, combined with established box models, can resolve several outstanding anomalies between model predictions and proxies for CO_2 and temperature. To advance further requires an improved modelling approach, for example, a continuous box model that can better represent physical climate and surface processes.

Acknowledgements

BJWM is funded by a University of Leeds Academic Fellowship and the UK Natural Environment Research Council (NERC) (NE/R010129/1). AJK is funded by a studentship from the NERC SPHERES Doctoral Training Partnership (NE/L002574/1). GAS and TML acknowledge funding through the NERC Biosphere Evolution, Transitions and Resilience project (NE/P013643/1), and through grants to GAS (NE/R010129/1) and TML (NE/N018508/1). The authors thank Dana Royer for providing proxy data and the GEOCARBSULF code. We also thank the reviewers of this work for their thoughtful comments.

Appendix A. Supplementary data

Supplementary data to this article can be found online at https://doi.org/10.1016/j.gr.2018.12.001.

References

Allegre, C.J., Louvat, P., Gaillardet, J., Meynadier, L., Rad, S., Capmas, F., 2010. The fundamental role of island arc weathering in the oceanic Sr isotope budget. Earth and Planetary Science Letters 292 (1–2), 51–56.

Arvidson, R.S., Mackenzie, F.T., Guidry, M., 2006. MAGic: a phanerozoic model for the geochemical cycling of major rock-forming components. American Journal of Science 306 (3), 135–190.

Arvidson, R.S., Mackenzie, F.T., Guidry, M.W., 2013. Geologic history of seawater: a MAGic approach to carbon chemistry and ocean ventilation. Chemical Geology 362, 87–304.

Bergman, N.M., Lenton, T.M., Watson, A.J., 2004. COPSE: A new model of biogeochemical cycling over Phanerozoic time. American Journal of Science 304, 397–437.

Bernard, S., et al., 2017. Burial-induced oxygen-isotope re-equilibration of fossil foraminifera explains ocean paleotemperature paradoxes. Nature Communications 8 (1), 1134.

Berner, R.A., 1987. Models for carbon and sulfur cycles and atmospheric oxygen: application to Paleozoic geologic history. American Journal of Science 287, 177–196.

Berner, R.A., 1991. A model for atmospheric CO_2 over Phanerozoic time. American Journal of Science 291, 339–376.

Berner, R.A., 1994. Geocarb II: a revised model of atmospheric CO_2 over Phanerozoic time. American Journal of Science 294, 56–91.

Berner, R.A., 2001. Modeling atmospheric O_2 over Phanerozoic time. Geochimica et Cosmochimica Acta 65 (5), 685–694.

Berner, R.A., 2004. The Phanerozoic Carbon Cycle: CO_2 and O_2. Oxford University Press, New York.

Berner, R.A., 2006. GEOCARBSULF: a combined model for Phanerozoic atmospheric O_2 and CO_2. Geochimica et Cosmochimica Acta 70, 5653–5664.

Berner, R.A., 2008. Addendum to "Inclusion of the Weathering of Volcanic Rocks in the GEOCARBSULF Model": (R. A. Berner, 2006, V. 306, p. 295-302). American Journal of Science 308, 100–103. https://doi.org/10.2475/01.2008.04.

Berner, R.A., 2009. Phanerozoic atmospheric oxygen: new results using the GEOCARBSULF model. American Journal of Science 309, 603–606.

Berner, R.A., Kothavala, Z., 2001. Geocarb III: a revised model of atmospheric CO_2 over Phanerozoic time. American Journal of Science 301, 182–204.

Berner, R.A., et al., 1983. The carbonate-silicate geochemical cycle and its effect on atmospheric carbon dioxide over the past 100 million years. American Journal of Science 283, 641–683.

Boyle, R.A., Dahl, T.W., Dale, A.W., Shields-Zhou, G.A., Zhu, M., Brasier, M.D., Canfield, D.E., Lenton, T.M., 2014. Stabilization of the coupled oxygen and phosphorus cycles by the evolution of bioturbation. Nature Geoscience 7, 671–676.

Brass, G.W., 1976. The variation of the marine $^{87}Sr/^{86}Sr$ ratio during Phanerozoic time: interpretation using a flux model. Geochemica et Cosmochemica Acta 40, 721–730.

Breecker, D.O., et al., 2010. Atmospheric CO_2 concentrations during ancient greenhouse climates were similar to those predicted for A.D. 2100. PNAS 107, 576–580.

Brune, S., Williams, S.E., Müller, R.D., 2017. Potential links between continental rifting, CO2 degassing and climate change through time. Nature Geoscience 10, 941–946.

Budyko, M.I., 1969. The effect of solar radiation variations on the climate of the Earth. Tellus 21 (5), 611–619.

Cao, W., Lee, C.-T.A., Lackey, J.S., 2017. Episodic nature of continental arc activity since 750 Ma: a global compilation. Earth and Planetary Science Letters 461, 85–95.

Cather, S.M., et al., 2009. Climate forcing by iron fertilization from repeated ignimbrite eruptions: the icehouse-silicic large igneous province (SLIP) hypothesis. Geosphere 5 (3), 315–324.

Caves, J.K., et al., 2016. Cenozoic carbon cycle imbalances and a variable weathering feedback. Earth and Planetary Science Letters 450, 152–163.

Cerling, T.E., 1984. The stable isotopic composition of modern soil carbonate and its relationship to climate. Earth and Planetary Science Letters 71 (1984), 229–240.

Charney, J., et al., 1979. Carbon Dioxide and Climate: A Scientific Assessment. National Research Council.

Coakley, J.A.C., Wielicki, B.A., 1979. Testing Energy Balance Climate Models. Journal of the Atmospheric Sciences 36, 2031–2039.

Conrad, C.P., 2013. The solid Earth's influence on sea level. Geological Society of America Bulletin 125, 1027–1052.

Cox, G.M., Halverson, G.P., Stevenson, R.K., Vokaty, M., Poirier, A., Kunzmann, M., Li, Z.-X., Denyszyn, S.W., Strauss, J.V., Macdonald, F.A., 2016. Continental flood basalt weathering as a trigger for Neoproterozoic Snowball Earth. Earth and Planetary Science Letters 446, 89–99.

Crowley, T.J., 1998. Tectonic Boundary Conditions for Climate Reconstructions. Oxford University Press, New York.

Dera, G., Brigaud, B., Monna, F., Laffont, R., Pucéat, E., Deconinck, J.-F., Pellenard, P., Joachimski, M.M., Durlet, C., 2011. Climatic ups and downs in a disturbed Jurassic world. Geology 39, 215–218.

Dessert, C., et al., 2003. Basalt weathering laws and the impact of basalt weathering on the global carbon cycle. Chemical Geology 202, 257–273.

Edmond, J.M., Huh, Y., 2003. Non-steady state carbonate recycling and implications for the evolution of atmospheric PCO_2. Earth and Planetary Science Letters 216 (1–2), 125–139.

Ernst, R.E., 2014. Large Igneous Provinces. Cambridge Univ. Press, Cambridge, U.K.

Evans, D., et al., 2018. Eocene greenhouse climate revealed by coupled clumped isotope-Mg/Ca thermometry. Proceedings of the National Academy of Sciences of the United States of America 115 (6), 1174–1179.

Falkowski, P.G., Katz, M.E., Milligan, A.J., Fennel, K., Cramer, B.S., Aubry, M.P., Berner, R.A., Novacek, M.J., Zapol, W.M., 2005. The rise of oxygen over the past 205 million years and the evolution of large placental mammals. Science 309, 2202–2204.

Foster, G.L., et al., 2017. Future climate forcing potentially without precedent in the last 420 million years. Nature Communications 8, 14845.

Francois, L.M., Walker, J.C.G., 1992. Modelling the Phanerozoic carbon cycle and climate: Constraints from the 87Sr/86Sr isotopic ratio of seawater. American Journal of Science 292, 81–135.

Friedrich, O., et al., 2012. Evolution of middle to Late Cretaceous oceans—a 55 m.y. record of Earth's temperature and carbon cycle. Geology 40 (2), 107–110.

Gabet, E.J., Mudd, S.M., 2009. A theoretical model coupling chemical weathering rates with denudation rates. Geology 37, 151–154.

Gaffin, S., 1987. Ridge volume dependence on seafloor generation rate and inversion using long term sealevel change. American Journal of Science 287, 596–611.

Gaillardet, J., Dupre´, B., Louvat, P., Alle`gre, C.J., 1999. Global silicate weathering and CO2 consumption rates deduced from the chemistry of large rivers. Chemical Geology 159, 3–30.

Galy, A., France-Lanord, C., Derry, L.A., 1999. The strontium isotopic budget of Himalayan Rivers in Nepal and Bangladesh. Geochimica et Cosmochimica Acta 63, 1905–1925.

Goddéris, Y., Donnadieu, Y., 2017. A sink- or a source-driven carbon cycle at the geological timescale? Relative importance of palaeogeography versus solid Earth degassing rate in the Phanerozoic climatic evolution. Geological Magazine 1–11.

Goddéris, Y., et al., 2012. Tectonic control of continental weathering, atmospheric CO_2, and climate over Phanerozoic times. Comptes Rendus Geoscience 344 (11—12), 652–662.

Goddéris, Y., et al., 2014. The role of palaeogeography in the Phanerozoic history of atmospheric CO_2 and climate. Earth-Science Reviews 128, 122–138.

Goddéris, Y., Donnadieu, Y., Carretier, S., Aretz, M., Dera, G., Macouin, M., Regard, V., 2017. Onset and ending of the late Palaeozoic ice age triggered by tectonically paced rock weathering. Nature Geoscience 10, 382–386.

Gregory, R.T., Taylor, H.P., 1981. An oxygen isotope profile in a section of Cretaceous oceanic crust, Samail Ophiolite, Oman: evidence for $\delta^{18}O$ buffering of the oceans by deep (>5 km) seawater-hydrothermal circulation at mid-ocean ridges. Journal of Geophysical Research: Solid Earth 86, 2737–2755. https://doi.org/10.1029/JB086iB04p02737.

Grossman, E.L., 2012. Oxygen isotope stratigraphy. The Geologic Time Scale. Elsevier, Boston, pp. 181–206.

Hansen, J.M., et al., 2008. Target atmospheric CO_2: where should humanity aim? Open Atmospheric Science Journal 2 (271–231).

Hansen, J., et al., 2013. Climate sensitivity, sea level and atmospheric carbon dioxide. Philosophical Transactions. Series A, Mathematical, Physical, and Engineering Sciences 371 (2001), 20120294.

Haq, B.U., 2014. Cretaceous eustasy revisited. Global and Planetary Change 113, 44–58.

Hartmann, J., Moosdorf, N., Lauerwald, R., Hinderer, M., West, A.J., 2014. Global chemical weathering and associated P-release — the role of lithology, temperature and soil properties. Chemical Geology 363, 145–163.

Hay, W.W., et al., 2006. Evaporites and the salinity of the ocean during the Phanerozoic: implications for climate, ocean circulation and life. Palaeogeography, Palaeoclimatology, Palaeoecology 240 (1–2), 3–46.

Hayes, J.M., Waldbauer, J.R., 2006. The carbon cycle and associated redox processes through time. Philosophical Transactions of the Royal Society B 361, 931–950.

Hilley, G.E., Porder, S., 2008. A framework for predicting global silicate weathering and CO_2 drawdown rates over geologic time-scales. Proceedings of the National Academy of Sciences of the United States of America 105 (44), 16855–16859.

Hoffman, P.F., Schrag, D.P., 2002. The snowball Earth hypothesis: testing the limits of global change. Terra Nova. vol. 14, pp. 129–155.

Hoffman, P.F., Kaufman, A.J., Halverson, G.P., Schrag, D.P., 1998. A neoproterozoic snowball earth. Science 281, 1342–1346.

Huntingford, C., Cox, P.M., 2000. An analogue model to derive additional climate change scenarios from existing GCM simulations. Climate Dynamics 16 (8), 575–586.

Huntingford, C., Booth, B.B.B., Sitch, S., Gedney, N., Lowe, J.A., Liddicoat, S.K., Mercado, L.M., Best, M.J., Weedon, G.P., Fisher, R.A., Lomas, M.R., Good, P., Zelazowski, P., Everitt, A.C., Spessa, A.C., Jones, C.D., 2010. IMOGEN: an intermediate complexity model to evaluate terrestrial impacts of a changing climate. Geoscientific Model Development 3 (2), 679–687.

Ikeda, T., Tajika, E., 1999. A study of the energy balance climate model with CO_2-dependent outgoing radiation: implication for the glaciation during the Cenozoic. Geophysical Research Letters 26, 349–352.

Inglis, G.N., et al., 2015. Descent towards the icehouse: Eocene sea surface cooling inferred from GDGT distributions. Paleoceanography, 29 https://doi.org/10.1002/2014PA002723.

Jacobson, A.D., Blum, J.D., 2003. Relationship between mechanical erosion and atmospheric CO_2 consumption in the New Zealand Southern Alps. Geology 31, 865–868.

Jasper, J.P., Hayes, J.M., 1990. A carbon isotope record of CO_2 levels during the late Quaternary. Nature 347, 462–464.

Jonas, A.S., Schwark, L., Bauersachs, T., 2017. Late Quaternary water temperature variations of the Northwest Pacific based on the lipid paleothermometers TEXH86, UK'37 and LDI. Deep Sea Research Part I: Oceanographic Research Papers 125, 81–93.

Kasting, J.F., 1989. Long-Term Stability of the Earth's climate. Paleogeogr. Paleoclimatol. Paleoecol. 75, 83–95.

Kelemen, P.B., Manning, C.E., 2015. Reevaluating carbon fluxes in subduction zones, what goes down, mostly comes up. Proceedings of the National Academy of Sciences of the United States of America 112, E3997–E4006.

Kennedy, M., et al., 2006. Late Precambrian oxygenation; Inception of the clay mineral factory. Science 311, 1446–1449.
Kirschvink, J.L., 1992. Late Proterozoic Low-latitude Global Glaciation: The Snowball Earth. Cambridge University Press.
Krause, A.J., Mills, B.J.W., Zhang, S., Planavsky, N.J., Lenton, T.M., Poulton, S.W., 2018. Stepwise oxygenation of the Paleozoic atmosphere. Nature Communications 9, 4081.
Kump, L.R., 1989. Alternative modeling approaches to the geochemical cycles of carbon, sulfur, and strontium isotopes. American Journal of Science 289, 390–410.
Kump, L.R., Arthur, M.A., 1997. Global Chemical Erosion during the Cenozoic: Weatherability Balances the Budgets. In: Ruddiman, W.F. (Ed.), Tectonic Uplift and Climate Change. Springer US, New York, pp. 399–426.
Lefebvre, V., et al., 2010. Did a Katian large igneous province trigger the Late Ordovician glaciation? Palaeogeography, Palaeoclimatology, Palaeoecology 296, 310–319.
Lenton, T.M., Watson, A.J., 2000a. Redfield revisited: I. Regulation of nitrate, phosphate and oxygen in the ocean. Global Biogeochemical Cycles 14, 225–248.
Lenton, T.M., Watson, A.J., 2000b. Redfield revisited: II. What regulates the oxygen content of the atmosphere? Global Biogeochemical Cycles 14, 249–268.
Lenton, T.M., Watson, A.J., 2004. Biotic enhancement of weathering, atmospheric oxygen and carbon dioxide in the Neoproterozoic. Geophysical Research Letters 31.
Lenton, T.M., Crouch, M., Johnson, M., Pires, N., Dolan, L., 2012. First plants cooled the Ordovician. Nature Geoscience 5 (2), 86–89.
Lenton, T.M., et al., 2018. COPSE reloaded: an improved model of biogeochemical cycling over Phanerozoic time. Earth Science Reviews 178, 1–28.
Li, G., Elderfield, H., 2013. Evolution of carbon cycle over the past 100 million years. Geochimica et Cosmochimica Acta 103, 11–25.
Lunt, D.J., Haywood, A.M., Schmidt, G.A., Salzmann, U., Valdes, P.J., Dowsett, H.J., 2010. Earth system sensitivity inferred from Pliocene modelling and data. Nature Geoscience 3, 60–64.
McArthur, J.M., Howarth, R.J., Shields, G.A., 2012. Chapter 7 - strontium isotope stratigraphy. The Geologic Time Scale. Elsevier, Boston, pp. 127–144.
McKenzie, N.R., et al., 2016. Continental arc volcanism as the principal driver of icehouse-greenhouse variability. Science 352, 444–447.
Merdith, A.S., et al., 2017. A full-plate global reconstruction of the Neoproterozoic. Gondwana Research 50, 84–134.
Mills, B.J.W., et al., 2011. Timing of Neoproterozoic glaciations linked to transport-limited global weathering. Nature Geoscience 4, 861–864.
Mills, B.J.W., et al., 2014. Changing tectonic controls on the long-term carbon cycle from Mesozoic to present. Geochemistry, Geophysics, Geosystems 15, 4866–4884.
Mills, B.J.W., et al., 2016. A modeling case for high atmospheric oxygen concentrations during the Mesozoic and Cenozoic. Geology 44, 1023–1026.
Mills, B.J.W., et al., 2017. Elevated CO_2 degassing rates prevented the return of Snowball Earth during the Phanerozoic. Nature Communications 8, 1110.
Misra, S., Froelich, P.N., 2012. Lithium isotope history of Cenozoic seawater: changes in silicate weathering and reverse weathering. Science 335, 818–823.
Nardin, E., Godderis, Y., Donnadieu, Y., Hir, G.L., Blakey, R.C., Puceat, E., Aretz, M., 2011. Modeling the early Paleozoic long-term climatic trend. Geological Society of America Bulletin 123, 1181–1192.
O'Brien, C.L., et al., 2017. Cretaceous sea-surface temperature evolution: constraints from TEX 86 and planktonic foraminiferal oxygen isotopes. Earth Science Reviews 172, 224–247.
Pagani, M., 2002. The alkenone-CO_2 proxy and ancient atmospheric carbon dioxide. Philosophical Transactions of the Royal Society of London A 360, 609–632.
Pearson, P.N., Palmer, M.R., 2000. Atmospheric carbon dioxide concentrations over the past 60 million years. Nature 406, 695–699.
Pohl, A., Donnadieu, Y., Le Hir, G., Buoncristiani, J.F., Vennin, E., 2014. Effect of the Ordovician paleogeography on the (in)stability of the climate. Climate of the Past 10 (6), 2053–2066.
Qin, W., Carlson, L.T., Armbrust, E.V., Devol, A.H., Moffett, J.W., Stahl, D.A., Ingalls, A.E., 2015. Confounding effects of oxygen and temperature on the TEX86 signature of marine Thaumarchaeota. Proceedings of the National Academy of Sciences of the United States of America 112, 10979–10984.
Raymo, M.E., Ruddiman, W.F., 1992. Tectonic forcing of late Cenozoic climate. Nature 359, 117–122.
Robinson, S.A., et al., 2017. Early Jurassic North Atlantic sea-surface temperatures from TEX86 palaeothermometry. Sedimentology 64, 215–230.
Ronov, A.B., 1993. Stratisfera—Ili Osadochnaya Obolochka Zemli (Kolichestvennoe Issledovanie), Moskva.
Rothman, D.H., et al., 2003. Dynamics of the Neoproterozoic carbon cycle. PNAS 100, 8124–8129.
Royer, D.L., 2001. Stomatal density and stomatal index as indicators of paleoatmospheric CO_2 concentration. Review of Palaeobotany and Palynology 114, 1–28.
Royer, D.L., 2014. Atmospheric CO_2 and O_2 during the Phanerozoic: tools. Patterns, and Impacts 251–267.
Royer, D.L., 2016. Climate sensitivity in the geologic past. Annual Review of Earth and Planetary Sciences 44, 277–293.
Royer, D.L., et al., 2004. CO_2 as a primary driver of Phanerozoic climate. GSA Today 14, 4–10.
Royer, D.L., et al., 2014. Error analysis of CO_2 and O_2 estimates from the long-term geochemical model GEOCARBSULF. American Journal of Science 314, 1259–1283.
Schachat, S.R., Labandeira, C.C., Saltzman, M.R., Cramer, B.D., Payne, J.L., Boyce, C.K., 2018. Phanerozoic pO_2 and the early evolution of terrestrial animals. Proceedings of the Biological Sciences 285.
Schouten, S., et al., 2002. Distributional variations in marine crenarchaeotal membrane lipids: a new tool for reconstructing ancient sea water temperatures? Earth and Planetary Science Letters 204, 265–274.
Shaviv, N.J., Veizer, J., 2004. Comment on "CO_2 as a primary driver of Phanerozoic climate". GSA today.
Shields, G.A., Mills, B.J.W., 2017. Tectonic controls on the long-term carbon isotope mass balance. Proceedings of the National Academy of Sciences of the United States of America 114, 4318–4323.
Snedden, J., Liu, C., 2010. A compilation of Phanerozoic sea-level change, coastal onlaps and recommended sequence designations. Am. Assoc. Pet. Geol. 40594.
Torres, M.A., et al., 2014. Sulphide oxidation and carbonate dissolution as a source of CO_2 over geological timescales. Nature 507, 346–349.
Trotter, J.A., et al., 2008. Did cooling oceans trigger Ordovician biodiversification? Evidence from conodont thermometry. Science 321, 550–554.
Van Cappellen, P., Ingall, E.D., 1994. Benthic phosphorus regeneration, net primary production, and ocean anoxia: a model of the coupled marine biogeochemical cycles of carbon and phosphorus. Paleoceanography 9, 677–692.
Van Cappellen, P., Ingall, E.D., 1996. Redox stabilisation of the atmosphere and oceans by phosphorus-limited marine productivity. Science 271, 493–496.
Van Der Meer, D.G., Zeebe, R.E., van Hinsbergen, D.J.J., Sluijs, A., Spakman, W., Torsvik, T.H., 2014. Plate tectonic controls on atmospheric CO_2 levels since the Triassic. Proceedings of the National Academy of Sciences 111 (12), 4380–4385.
Veizer, J., Prokoph, A., 2015. Temperatures and oxygen isotopic composition of Phanerozoic oceans. Earth Science Reviews 146, 92–104.
Veizer, J., et al., 1999. $^{87}Sr/^{86}Sr$, delta^{13}C and delta^{18}O evolution of Phanerozoic seawater. Chemical Geology 161, 59–88.
Veizer, J., et al., 2000. Evidence for decoupling of atmospheric CO_2 and global climate during the Phanerozoic Eon. Nature 408, 698–701.
Visser, K., et al., 2003. Magnitude and timing of temperature change in the Indo-Pacific warm pool during deglaciation. Nature 421, 152–155.
Volk, T., 1989. Sensitivity of climate and atmospheric CO_2 to deep-ocean and shallow-ocean carbonate burial. Nature 337, 637–939.
Walker, J.C.G., Hays, P.B., Kasting, J.F., 1981. A negative feedback mechanism for the long-term stabilization of Earth's surface temperature. Journal of Geophysical Research 86, 9776–9782.
West, A.J., 2012. Thickness of the chemical weathering zone and implications for erosional and climatic drivers of weathering and for carbon-cycle feedbacks. Geology 40, 811–814.
West, A.J., et al., 2005. Tectonic and climatic controls on silicate weathering. Earth and Planetary Science Letters 235, 211–228.
von Willenbring, J.K., Blanckenburg, F.v., 2010. Long-term stability of global erosion rates and weathering during late-Cenozoic cooling. Nature 465, 211–214.
Wold, C.N., Hay, W.W., 1990. Estimating ancient sediment fluxes. American Journal of Science 290, 1069–1089.
Young, S.A., et al., 2009. A major drop in seawater $^{87}Sr/^{86}Sr$ during the Middle Ordovician (Darriwilian): links to volcanism and climate? Geology 37, 951–954.
Zachos, J., et al., 2001. Trends, rhythms and aberrations in global climate 65 Ma to present. Science 292, 686–693.
Zachos, J.C., Dickens, G.R., Zeebe, R.E., 2008. An early Cenozoic perspective on greenhouse warming and carbon-cycle dynamics. Nature 451, 279–283. https://doi.org/10.1038/nature06588.
Zhang, Y.G., Pagani, M., Liu, Z., Bohaty, S.M., Deconto, R., 2013. A 40-million-year history of atmospheric CO(2). Philosophical Transactions. Series A, Mathematical, Physical, and Engineering Sciences 371 (20130096).
Zhang, Y.G., et al., 2014. A 12-million-year temperature history of the tropical pacific ocean. Science 344, 84–87.

Benjamin J. W. Mills is an Academic fellow at the University of Leeds. He received a Master's degree in mathematics in 2008 and a PhD in biogeochemical modelling in 2013, both awarded by the University of East Anglia. His work focuses on the evolution of Earth's surface environment over geological time, and specifically on the processes controlling atmospheric CO$_2$ and O$_2$ levels. He has rewritten and extended current biogeochemical models as well as developing novel theoretical frameworks to test hypotheses in geochemistry and evolution.

Alexander J. Krause is a PhD candidate at the University of Leeds. His PhD research involves building biogeochemical box models, as well as undertaking geochemical analyses of sedimentary rocks, to generate estimates of atmospheric oxygen levels on Earth over the last billion years. His underlying aim is to understand the key processes which have driven Earth to a habitable state for multicellular life, with an eye on how this information could be employed in the search for life on other planets.

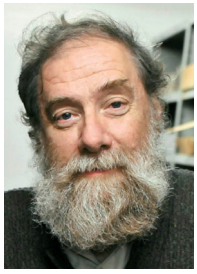

Christopher R. Scotese retired from teaching at the University of Texas, Arlington, Department of Earth and Environmental Sciences in 2013. He is now a Research Associate at the Field Museum of Natural History and an Adjunct Professor in the Department of Earth and Environmental Sciences, Northwestern University. He continues to collaborate with several research groups on topics concerning the history of the Earth System, but his main focus is a book entitled: "Earth History, the Evolution of the Earth System". He is the coauthor of >100 scientific publications, and his maps and animations have been used in numerous geological textbooks, scientific research papers, and are on display in museums worldwide.

Daniel J. Hill is a lecturer in global change modelling in the School of Earth and Environment at the University of Leeds. As a paleoclimate modeller, he investigates the mechanisms and impacts of climate change across a wide range of timescales through Earth history. Having spent much of his career simulating the climate of the Pliocene Epoch, including the ocean, cryosphere, biosphere and paleogeographic change, he is now studying the climatic drivers of the Permo-Triassic mass extinction and the impact of climate on ancient civilizations and many of the climatic changes in between.

Graham A. Shields received his PhD from the ETH Zurich in 1997, since which time he has worked in France, Canada, Australia, Germany and the UK on diverse aspects of Earth system evolution and sedimentary geochemistry. Since 2013 he has been professor of chemical geology at University College London where his research focus aims at a better understanding of the coupled oxygen and carbon cycles on long time scales. Currently, he is the scientific coordinator of the Biosphere Evolution, Transitions & Resilience programme, funded by UK's Natural Environmental Research Council.

Timothy M. Lenton is Director of the Global Systems Institute and Chair in Climate Change and Earth System Science at the University of Exeter. He has a BA in Natural Sciences from the University of Cambridge (1994) and obtained his PhD degree in Environmental Sciences from the University of East Anglia in 1998. His research focuses on the coupled evolution of life and the planet and on climate change tipping points and early warning methods. He developed the COPSE model as a framework for testing hypotheses about biogeochemical cycling and Earth system functioning in deep time.